


# Super-broadband geometric phase devices based on circular polarization converter with mirror symmetry

Cite as: Appl. Phys. Lett. **119**, 101103 (2021); <https://doi.org/10.1063/5.0060647>

Submitted: 21 June 2021 • Accepted: 24 August 2021 • Published Online: 08 September 2021

 Wan Chen, Yang Yu, Quanquan Mu, et al.



View Online



Export Citation



CrossMark

## ARTICLES YOU MAY BE INTERESTED IN

[Broadband low-frequency sound absorbing metastructures based on impedance matching coiled-up cavity](#)

Applied Physics Letters **119**, 101901 (2021); <https://doi.org/10.1063/5.0061012>

[Molecular passivation of MAPbI<sub>3</sub> perovskite films follows the Langmuir adsorption rule](#)

Applied Physics Letters **119**, 101101 (2021); <https://doi.org/10.1063/5.0061818>

[Reproducible coherence characterization of superconducting quantum devices](#)

Applied Physics Letters **119**, 100501 (2021); <https://doi.org/10.1063/5.0060370>

Lock-in Amplifiers  
up to 600 MHz



Zurich  
Instruments



# Super-broadband geometric phase devices based on circular polarization converter with mirror symmetry

Cite as: Appl. Phys. Lett. **119**, 101103 (2021); doi: 10.1063/5.0060647

Submitted: 21 June 2021 · Accepted: 24 August 2021 ·

Published Online: 8 September 2021



View Online



Export Citation



CrossMark

Wan Chen,<sup>1,2</sup>  Yang Yu,<sup>1,2</sup> Quanquan Mu,<sup>1,2,a)</sup> Juan Campos,<sup>3</sup> Qidong Wang,<sup>1,a)</sup> Shixiao Li,<sup>1,2</sup> Shiyuan Zhang,<sup>1,2</sup> and Li Xuan<sup>1,2</sup>

## AFFILIATIONS

<sup>1</sup>State Key Laboratory of Applied Optics, Changchun Institute of Optics, Fine Mechanics and Physics, Chinese Academy of Sciences, Changchun 130033, China

<sup>2</sup>University of Chinese Academy of Sciences, Beijing 100049, China

<sup>3</sup>Grup d'Òptica, Physics Department, Universitat Autònoma de Barcelona, Bellaterra 08193, Spain

<sup>a)</sup>Authors to whom correspondence should be addressed: [muquanquan@ciomp.ac.cn](mailto:muquanquan@ciomp.ac.cn) and [qdwang@ciomp.ac.cn](mailto:qdwang@ciomp.ac.cn)

## ABSTRACT

We propose a simple implementation to obtain super-broadband geometric phase devices (GPD) by means of circular polarization converter (CPC) with mirror symmetry. We demonstrate that the best choice of wideband GPDs and CPCs is a mirror symmetric structure. Based on a two-rotation model on the Poincaré sphere, optimization parameters and time are significantly reduced. The CPC can be extended to super-broadband GPD, such as polarization gratings (PGs), by using geometric phase holography. We simulate diffraction efficiencies of the super-broadband PGs. In the normal incident case, the diffraction efficiency is over 99% in 420–945 nm, and in the oblique incident case, the first-order diffraction efficiency is over 90% in the range of  $\pm 30^\circ$ . The super-broadband GPDs show potential advantages in wide color display and spectral imaging.

© 2021 Author(s). All article content, except where otherwise noted, is licensed under a Creative Commons Attribution (CC BY) license (<http://creativecommons.org/licenses/by/4.0/>). <https://doi.org/10.1063/5.0060647>

Polarization control is one of the significant means of optical control. Since the Geometric phase<sup>1</sup> was proposed, polarization control has been extended to a new generation, and the demand for wide-band has become increasingly inevitable. Many kinds of geometric phase devices (GPDs)<sup>2–5</sup> have been used in optical systems. However, it is highly desirable that most applications need GPDs with high diffraction efficiency, broad bandwidth, and wide field angles. Dual-twist achromatic polarization gratings (PGs)<sup>6</sup> show a broader bandwidth than the single-layer non-twist PGs. Wu *et al.*<sup>7</sup> produced broadband wide-view PGs with three-layer self-aligned multi-twist structures, which demonstrated the feasibility of multi-twist structures for broadband and large-view angles. Xiong *et al.*<sup>8</sup> reviewed the performance improvement of the above two multi-twist structures in terms of bandwidth and viewing angles and gave a visual explanation. Although these reports show good broadband properties, no one has discussed what kind of multi-twist structure is a better choice for constructing GPDs. It is worth seeking a simpler and more effective theory to provide guidance on the design and fabrication of GPDs.

In this Letter, we propose a simple implementation of a super-broadband GPD, namely, a broadband circular polarization converter (CPC) combined with an optical axis pattern. First, we consider using the self-aligned multi-twist structure<sup>9</sup> with mirror symmetry to produce broadband CPCs. Then, based on the proposed two-rotation model of twisted liquid crystal (LC) layers on the Poincaré sphere, we demonstrate the advantage in achromatism of a CPC with mirror symmetry over an asymmetric one and optimize fast to get two kinds of broadband CPCs. Finally, the diffraction efficiencies of normal incidence of the broadband PGs generated by broadband CPCs are simulated, and the angular response of the typical wavelength is observed.

Generally, a GPD satisfying a half-wave condition can be regarded as a patterned half-wave plate (HWP), whose operation principle can be explained by following Jones matrix:<sup>7</sup>

$$J'_{\pm} = \frac{1}{\sqrt{2}} \begin{pmatrix} \cos 2\phi & \sin 2\phi \\ \sin 2\phi & -\cos 2\phi \end{pmatrix} \begin{pmatrix} 1 \\ \pm i \end{pmatrix} = \frac{1}{\sqrt{2}} \begin{pmatrix} 1 \\ \mp i \end{pmatrix} \exp(\pm 2i\phi). \quad (1)$$

For a left-handed circularly polarized (LCP) input light, the output changes to a right-handed circularly polarized (RCP) with an extra Geometric phase  $2\phi$ , where  $\phi$  is the azimuthal angle of the optical axis. The optical axis orientations are determined by the desired patterns according to the GPDs' optical function, such as PGs as shown in Fig. 1(c) and polarization lenses (PLs) as shown in Fig. 1(d). Different geometric phase holography methods have been reported to create the desired LC orientation patterns, including direct writing,<sup>10</sup> and the Digital Micro-mirror Device based on lithography<sup>11</sup> and the photo-alignment technique.<sup>2,10</sup> As we all know, when the GPDs' birefringent layer meets the half-wave retardation, there exist only first orders, which is essentially because a HWP can switch between LCP and RCP perfectly. Similarly, as shown in Fig. 1(b), a broadband CPC should switch between LCP and RCP perfectly in wideband. Broadband CPCs combined with diverse LC orientation patterns will produce broadband GPDs, as shown in Figs. 1(b)–1(f). Figures 1(e) and 1(f) show the schematic diagram of super-broadband PGs in top-view and side-view. The diffraction behavior is shown in Fig. 1(g).

We select the mirror symmetric self-aligned multi-twist structure to design the CPCs as shown in Fig. 1(a). Here, the mirror symmetric structure means that the twisted angles and thicknesses are mirror symmetric about the overall thickness center (red dot and dash line) of polymeric LC layers. The first layer is aligned by the alignment layer,

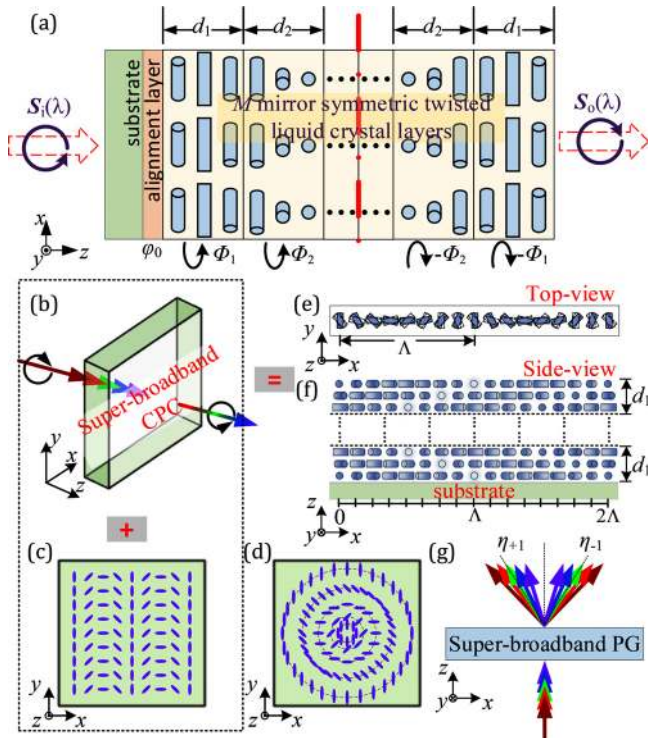


**FIG. 1.** (a) Illustration of the mirror symmetric self-aligned multi-twist structure, with one substrate, one alignment layer, and  $M$  twisted layers. The LC layers show mirror symmetry about the center of the total thicknesses. (b) Ideal polarization conversion of super-broadband CPCs. The optical axis orientations of PGs (c) and PLs (d) generated by geometric phase hologram. A schematic diagram of the super-broadband PGs in top-view (e) and side-view (f). (g) Diffraction behavior of a super-broadband PG.

and the subsequent layers are oriented by the prior one. To explain why mirror-symmetric structures are chosen for the CPCs, we first need to study the polarization state modulation effect of single- and multi-twist LC layers on broadband incident polarization light.

It is perfectly reasonable in most cases to assume that the LC layer is not absorbing, and in consequence to describe a single-twist LC layer, we will use the  $3 \times 3$  lower part of the Mueller matrix<sup>12</sup> that is given by

$$\mathbf{M} = \mathbf{R}(-\Phi) \begin{pmatrix} 1 - 2\frac{\Phi^2}{X^2} \sin^2 X & \frac{\Phi}{X} \sin(2X) & \frac{\Phi\Gamma}{X^2} \sin^2 X \\ -\frac{\Phi}{X} \sin(2X) & \cos(2X) & \frac{\Gamma}{2X} \sin(2X) \\ \frac{\Phi\Gamma}{X^2} \sin^2 X & -\frac{\Gamma}{2X} \sin(2X) & 1 - 2\frac{\Gamma^2}{(2X)^2} \sin^2 X \end{pmatrix}, \quad (2)$$

where initial director of LC is along the  $x$ -axis, as shown in Fig. 1(a),  $\Phi$  is the twist angle,  $\Gamma$  is the phase retardation given by  $\Gamma = 2\pi\Delta n \cdot d/\lambda$  for wavelength  $\lambda$ , and  $X = \text{sqrt}(\Phi^2 + (\Gamma/2)^2)$ . We define that  $\Phi > 0$  means left-handed twist, and  $\Phi < 0$  means right-handed twist.  $\mathbf{R}(\Phi)$  is the Mueller rotation matrix, which is given by following equation:

$$\mathbf{R}(\Phi) = \begin{pmatrix} \cos(2\Phi) & \sin(2\Phi) & 0 \\ -\sin(2\Phi) & \cos(2\Phi) & 0 \\ 0 & 0 & 1 \end{pmatrix}. \quad (3)$$

When  $\Phi > 0$ , it means that the Stokes vector space rotates  $2\Phi$  counter-clockwise around the  $S_3$ -axis, which corresponds to the coordinate rotation transformation of the Jones matrix.<sup>12</sup> More generally, considering the angle  $\varphi_0$  between  $x$ -axis and the initial director of LC, the Mueller matrix through a single-twist LC layer is

$$\mathbf{M}(\varphi_0) = \mathbf{R}(-\varphi_0) \cdot \mathbf{M} \cdot \mathbf{R}(\varphi_0). \quad (4)$$

Ramachandran and Ramaseshan<sup>13</sup> have shown that the eigenstates are no longer two linear polarized states, but two ellipsoid states when a beam of light propagates in a medium exhibiting both optical activity and birefringence simultaneously. Subsequently, a Poincaré sphere representation method<sup>14,15</sup> was proposed that the evolution of the state of polarization (SOP) for a single-twist LC layer was associated with a spherical cycloid. Here, we derive a more compact and powerful method that can obtain optical properties of a single-twist LC layer simply by two rotations on the Poincaré sphere. Once the optical properties of the single-twist LC layer are understood, the optical properties of the multi-twist layers can also be determined. In this Letter, we define the North Pole as RCP and the South Pole as LCP.

Now, we rewrite the Eq. (4) as follows:

$$\mathbf{M}(\varphi_0) = \mathbf{R}(-\varphi_0)\mathbf{R}(-\Phi)\mathbf{P}(-\rho)\mathbf{Q}(2X)\mathbf{P}(\rho)\mathbf{R}(\varphi_0), \quad (5)$$

$$\mathbf{P}(\rho) = \begin{pmatrix} \cos\rho & 0 & \sin\rho \\ 0 & 1 & 0 \\ -\sin\rho & 0 & \cos\rho \end{pmatrix}, \quad (6)$$

$$\mathbf{Q}(2X) = \begin{pmatrix} 1 & 0 & 0 \\ 0 & \cos(2X) & \sin(2X) \\ 0 & -\sin(2X) & \cos(2X) \end{pmatrix}, \quad (7)$$

where  $\tan \rho = 2\Phi/\Gamma$  and  $\rho$  determines the latitude of the eigenstates on the Poincaré sphere. The longitudes of the eigenstates are determined by the azimuthal angle  $\varphi_0$  of the LC directors. As shown in Fig. 2, the two eigenstates are orthogonal, and they constitute one diameter of the Poincaré sphere. Here, we select one of the two eigenstates, C (with the longitude  $\rho$  and latitude  $2\varphi_0$ ), as a reference point. The matrices of Eqs. (5)–(7) all have the form of coordinate rotation. Note that  $\mathbf{P}(\rho)\mathbf{R}(\varphi_0)$  is make the  $S_1$ -axis along with ray OC. Therefore, based on the reversibility between transformation of coordinate and SOPs' rotation, we can draw a following conclusion. As shown in Fig. 2, for the single-twist LC layer, any incident SOP first rotates  $2X$  clockwise around the line between the eigenstate C and the center O of the Poincaré sphere, then rotates  $2\Phi$  counterclockwise around the  $S_3$ -axis, and reaches the outgoing SOP. The two rotations have physical meanings.  $2X$  is the equivalent retardation, which dominates the broadening of the “polarization dispersion” on the Poincaré sphere. The second rotation angle is determined only by  $2\Phi$ , which just changes the azimuth of the SOPs, but has no effect on the polarization dispersion. What is more, the two-rotation model can be easily implemented using geometry software. By adjusting any parameter arbitrarily to observe the response of the intermediate and final SOPs over the whole wideband, the final parameters are decided. Note that the two-rotation model is no longer a simple tool to finally present the polarization states evolution path, but has the function of implementing dynamic optimization. Next, we will use the visual model to design broadband CPCs.

We declare that the best choice is a mirror symmetric structure for broadband CPCs [see Fig. 1(a)]. Figure 3 illustrates superiority in waveband of the mirror-symmetric structure over the non-mirror symmetric structure. Rainbow arc  $S_{o1}$  (or  $S'_{o1}$ ) represents a set of Stokes vectors after a wideband RCP (or LCP) input light passes through a single-twist LC layer with thickness  $d_1$  (or  $d'_1$ ).  $I_1$  (or  $I'_1$ ) represents evolution of SOPs RCP/LCP with a wavelength of 532 nm. When the LCP/RCP propagates through a single-twist LC structure, the outgoing SOPs create the polarization dispersion effect as shown in Figs. 3(c) and 3(d) with rainbow color. Different thicknesses and twisted angles result in different degrees of polarization dispersion. Generally, the larger the thickness is, the more dispersed the outgoing SOPs are. As shown in Figs. 3(a) and 3(c), the low degree of overlap

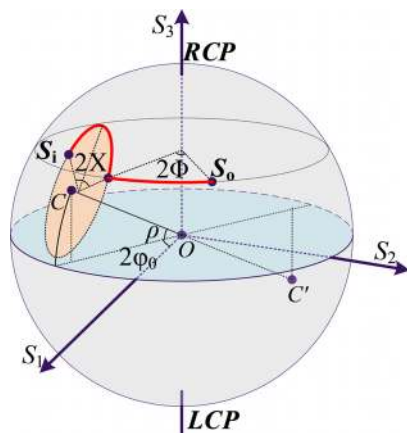


FIG. 2. Two-rotation model for a single-twist LC layer.

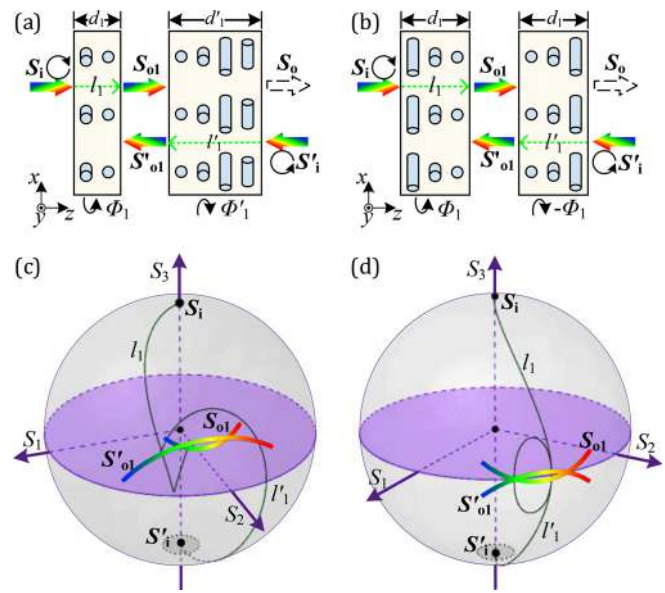


FIG. 3. Illustration of superiority in waveband of the mirror symmetric structure. (a) and (c) Non-mirror symmetric structures with thicknesses  $d_1 < d'_1$  and twisted angles  $\Phi_1 \neq -\Phi'_1$ . (b) and (d) Mirror symmetric structures.

between  $S_{o1}$  and  $S'_{o1}$  means that  $S_{o1}$  cannot return to the South Pole (LCP) by a reversible path. In brief, polarization dispersion does not form mutual compensation. It is obvious that mirror symmetric structures as shown in Figs. 3(b) and 3(d) are wider than non-mirror symmetric ones in bandwidth.

To obtain the super-broadband GPDs and CPCs, we chose four-twist LC layers. Figure 4(a) shows a four-layer broadband CPC with mirror symmetry, which satisfies  $\Phi_4 = -\Phi_1$ ,  $\Phi_3 = -\Phi_2$ ,  $d_4 = d_1$ , and  $d_3 = d_2$ . The four twist angles from first to fourth are designed in two combinations,  $++--$  (or  $--++$ ) and  $+-+-$  (or  $-+-+$ ), where

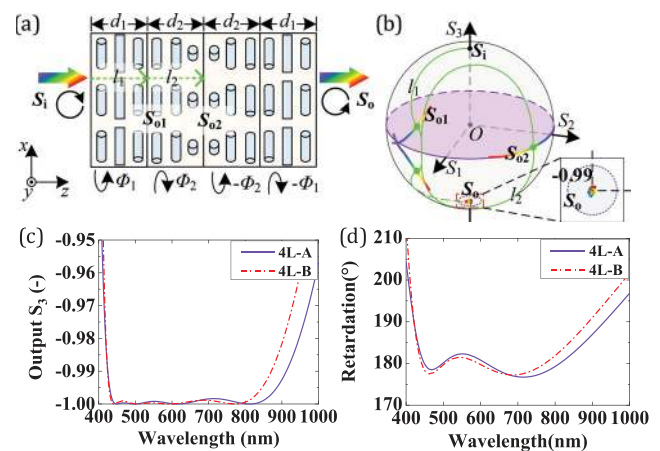


FIG. 4. (a) Four-layer broadband CPCs with mirror symmetry. (b) Dynamic monitoring SOPs on the Poincaré sphere. (c) Output  $S_3$  and (d) retardation angles of final  $S_o$  in the case of RCP input light.

“+” and “-” represent left handed and right handed, respectively. We just need to optimize the parameters  $\Phi_1, \Phi_2, d_1,$  and  $d_2$ . In Figs. 4(a) and 4(b),  $S_{o1}/S_{o2}$  represents a set of Stokes vectors after a wideband RCP input light passes through the first one/two LC layers.  $l_1/l_2$  represents the evolution of SOPs when an input beam with a wavelength of 532 nm passes through the first/second LC layer. We use the two-rotation model to track the evolution of SOPs of the four-twist LC layers on the Poincaré sphere in real time. Due to the mirror symmetry, the visual optimization criterion is to make the outgoing SOPs arc of the second layer  $S_{o2} = [S_1(\lambda), S_2(\lambda), S_3(\lambda)]^T$  fall all near the equator of the Poincaré sphere as shown with rainbow color in Fig. 4(b). In other words, make sure  $|S_3(\lambda)|$  of  $S_{o2}$  are less than 0.1, so that the outgoing normalized Stokes parameter values  $|S_3(\lambda)|$  of  $S_o$  are greater than 0.98. We listed two good designs 4L-A and 4L-B as shown in Table I. All the designs use the same  $\Delta n = 0.128 + 8390/\lambda^2$ , where the unit of  $\lambda$  is nanometer. Considering the dispersion, four-layer BPCs can achieve the wideband polarization conversion from 420 to 945 nm, as shown in Fig. 4(c). Meanwhile, the retardation angles are all between  $176.3^\circ$  and  $190^\circ$ . Note that it is easy to theoretically change the wavelength ranges only by scaling the thicknesses without changing the twisted angles, and this is also true for different LC materials with different birefringence  $\Delta n$ , which is decided by  $\Gamma = 2\pi\Delta n \cdot d/\lambda$ .

As shown in Figs. 1(b)–1(f), the parameters of four-layer super-broadband CPCs can be used in super-broadband GPDs, such as PGs or PLs. Reference 7 has provided the method to fabricate multi-twist PGs. The twisted angles can be controlled by adjusting the proportion of the chiral materials and the reactive mesogen, and the thicknesses can be precisely controlled by coating several reactive mesogen layers.

We use the rigorous coupled wave analysis (RCWA)<sup>16</sup> to simulate the diffraction efficiency of four-layer super-broadband PGs with parameters of 4L-A, as shown in Table I. The grating period was set to a relatively large value,  $15 \mu\text{m}$ , satisfying the condition in the Raman–Nath regime. Figure 5 shows diffraction efficiency curves of four-layer super-broadband PGs at normal incidence. The result shows that the first-order diffraction efficiencies of the structure are over 99% from 420 to 945 nm and almost the same for RCP and LCP incident light in the normal incident case. We compare the results with the three-layer multi-twist broadband PGs and the two-layer ones,<sup>6,7</sup> and here, we use the same birefringence  $\Delta n = 0.128 + 8390/\lambda^2$  for scaling the thicknesses. The specific parameters are three-layer ( $d_1 = 1.103 \mu\text{m}, d_2 = 1.485 \mu\text{m}, d_3 = 0.99 \mu\text{m}, \Phi_1 = -69.4^\circ, \Phi_2 = 3.7^\circ,$  and  $\Phi_3 = 64^\circ$ ) and two-layer ( $d_1 = 1.5 \mu\text{m}, d_2 = 1.5 \mu\text{m}, \Phi_1 = -70^\circ,$  and  $\Phi_2 = 70^\circ$ ). The four-layer super-broadband PGs show high diffraction efficiency in the ultra-wideband ranges. Assume that the thicknesses and twisted angles of four-layer super-broadband PGs can be accurately controlled, the diffraction efficiency will be determined only by the following equation:<sup>17</sup>

$$\eta_{\pm 1} = \frac{1}{2}(1 \mp S_3), \tag{8}$$

TABLE I. Design parameters of super-broadband CPCs.

Designs	$\varphi_0(^\circ)$	$d_1(\mu\text{m})$	$\Phi_1(^\circ)$	$d_2(\mu\text{m})$	$\Phi_2(^\circ)$
4L-A	Optional	2.31	103.7	1.11	-68.3
4L-B	Optional	2.22	31.6	0.98	84.4

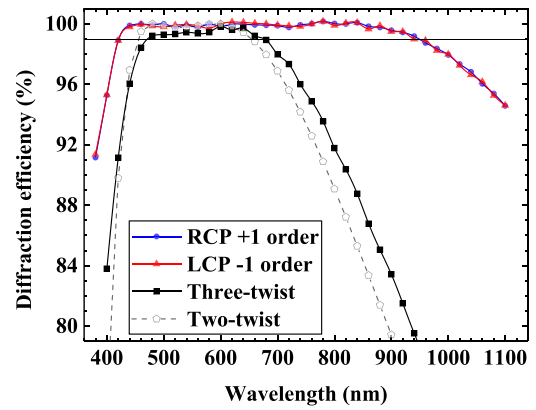


FIG. 5. Diffraction efficiency curves of four-layer super-broadband PGs generated by 4L-A CPCs, three-layer multi-twist broadband PGs, and two-layer PGs at normal incidence.

where  $S_3$  is the normalized Stokes parameter corresponding to polarization conversion efficiency of CPCs, as shown in Fig. 4(c). Polarization conversion efficiency refers to the proportion of LCP (or RCP) components of a beam of RCP (or LCP) passing through a broadband CPC.

The diffraction efficiencies of three typical wavelengths at different incidence angles are calculated using RCWA. Figure 6 displays angular response of the four-layer super-broadband PGs. The three main wavelengths are R = 630 nm, G = 530 nm, and B = 460 nm. The first-order diffraction efficiency can reach 90% in the range of  $\pm 30^\circ$ , which proves that this kind of super-broadband PG has wide-view properties at the same time.

In summary, we propose a simple implementation to design super-broadband GPDs. We develop a two-rotation model to dynamically trace the polarization conversion properties of multi-twist LC layers. Then, we demonstrate the advantage in achromatism of a CPC with mirror symmetry over an asymmetric one. Moreover, mirror symmetric structures can significantly reduce optimization complexity. The optimized four-twist wideband CPCs combined with geometric phase holography can easily generate ultra-wideband GPDs. The super-broadband GPDs show potential advantages in wide color display, optical communication, and spectral imaging. This simple design method probably become the main means for the design of GPDs with wideband and large view angle.

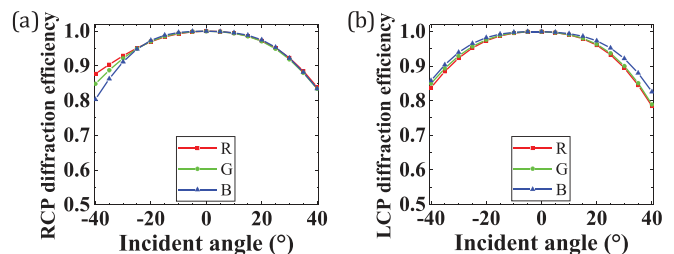


FIG. 6. First-order diffraction efficiency curves of four-layer super-broadband PGs at oblique incidence.

This work was supported by the CAS Inter-disciplinary Innovation Team, National Natural Science Foundation of China (Grant Nos. 11974345, 61975202, U2030101, 11604327, and 61775212) and the Chinese Academy of Sciences President's International Fellowship Initiative Grant No. 2020VTA0004.

#### DATA AVAILABILITY

The data that support the findings of this study are available within the article.

#### REFERENCES

- <sup>1</sup>M. Martinelli and P. Vavassori, "A geometric (Pancharatnam) phase approach to the polarization and phase control in the coherent optics circuits," *Opt. Commun.* **80**, 166 (1990).
- <sup>2</sup>G. P. Crawford, J. N. Eakin, M. D. Radcliffe, A. Callan-Jones, and R. A. Pelcovits, "Liquid-crystal diffraction gratings using polarization holography alignment techniques," *J. Appl. Phys.* **98**, 123102 (2005).
- <sup>3</sup>C. Provenzano, P. Pagliusi, and G. Cipparrone, "Highly efficient liquid crystal based diffraction grating induced by polarization holograms at the aligning surfaces," *Appl. Phys. Lett.* **89**, 121105 (2006).
- <sup>4</sup>T. Zhan, Y. H. Lee, and S. T. Wu, "High-resolution additive light field near-eye display by switchable Pancharatnam–Berry phase lenses," *Opt. Express* **26**, 4863 (2018).
- <sup>5</sup>L. Li, J. Kim, S. Shi, and M. J. Escuti, "Color-selective geometric phase lens for apochromatic lens system," *Proc. SPIE* **11472**, 1147219 (2020).
- <sup>6</sup>C. Oh and M. J. Escuti, "Achromatic diffraction from polarization gratings with high efficiency," *Opt. Lett.* **33**, 2287 (2008).
- <sup>7</sup>J. Zhou, T. Zhan, J. Xiong, and S. T. Wu, "Broadband wide-view Pancharatnam–Berry phase deflector," *Opt. Express* **28**, 4921 (2020).
- <sup>8</sup>J. Xiong and S. T. Wu, "Planar liquid crystal polarization optics for augmented reality and virtual reality: From fundamentals to applications," *eLight* **1**, 1–20 (2021).
- <sup>9</sup>R. K. Komanduri, K. F. Lawler, and M. J. Escuti, "Multi-twist retarders: Broadband retardation control using self-aligning reactive liquid crystal layers," *Opt. Express* **21**, 404 (2013).
- <sup>10</sup>J. Kim, Y. Li, M. N. Miskiewicz, C. Oh, M. W. Kudenov, and M. J. Escuti, "Fabrication of ideal geometric-phase holograms with arbitrary wavefronts," *Optica* **2**, 958 (2015).
- <sup>11</sup>W. Hao, H. Wei, H. Hu, X. Lin, Z. Ge, J. W. Choi, V. Chigrinov, and Y. Lu, "Arbitrary photo-patterning in liquid crystal alignments using DMD based lithography system," *Opt. Express* **20**, 16684 (2012).
- <sup>12</sup>D. K. Yang and S. T. Wu, *Fundamentals of Liquid Crystal Devices*, 2nd ed. (John Wiley & Sons, Ltd, 2015), pp. 102–110.
- <sup>13</sup>G. N. Ramachandran and S. Ramaseshan, "Magneto-optic rotation in birefringent media—application of the Poincaré sphere," *J. Opt. Soc. Am.* **42**, 49 (1952).
- <sup>14</sup>J. E. Bigelow and R. A. Kashnow, "Poincaré sphere analysis of liquid crystal optics," *Appl. Opt.* **16**, 2090 (1977).
- <sup>15</sup>Z. Zhuang, Y. J. Kim, and J. S. Patel, "Achromatic linear polarization rotator using twisted nematic liquid crystals," *Appl. Phys. Lett.* **76**, 3995 (2000).
- <sup>16</sup>J. Xiong and S. T. Wu, "Rigorous coupled-wave analysis of liquid crystal polarization gratings," *Opt. Express* **28**, 35960 (2020).
- <sup>17</sup>J. Kim, C. Oh, M. J. Escuti, L. Hosting, and S. Serati, "Wide-angle nonmechanical beam steering using thin liquid crystal polarization gratings," *Proc. SPIE* **7093**, 709302 (2008).